The Influence of Meltwater on Phytoplankton Blooms Near the Sea-Ice Edge

Conner W. Lester[1,2], T. J. W. Wagner[1], Dylan E. McNamara[1], M.R. Cape[3]

[1]Department of Physics and Physical Oceanography/Center for Marine Science, University of North Carolina Wilmington, Wilmington, NC, United States
[2]Division of Earth and Ocean Sciences, Nicholas School of the Environment, Center for Nonlinear and Complex Systems, Duke University, Durham, NC, United States
[3]Applied Physics Laboratory, University of Washington, Seattle, WA, United States

Key Points:

- Observations show that sea-ice edge phytoplankton blooms are closely correlated with sea-ice meltwater.
- We present an idealized model of phytoplankton dynamics where the influence of meltwater and sunlight is parameterized in phytoplankton growth and death rates.
- Model output qualitatively matches data of phytoplankton blooms in Fram Strait, highlighting the role of meltwater in bloom development.

Corresponding author: Conner W. Lester, conner.lester@duke.edu

Abstract

Annual sea-ice edge phytoplankton blooms occur throughout the Arctic during the spring melt period. Our study considers how phytoplankton spring blooms may depend on sea-ice meltwater. We extend the classic Fisher reaction-diffusion equation to consider a time- and space-varying death rate that represents the role of meltwater in the system. Our results indicate that blooms peak at a characteristic distance from the ice edge where *(i)* meltwater is still concentrated enough to stratify the upper ocean such that the phytoplankton are confined near the surface and *(ii)* phytoplankton have been exposed to sufficient sunlight to allow for maximum growth. The results are qualitatively similar to satellite data of a large bloom observed in Fram Strait in May 2019. Our findings support the idea that sea-ice meltwater is of central importance for Arctic phytoplankton blooms.

Plain Language Summary

In the Arctic, each spring the appearance of the sun awakens the regions ecosystem. In particular, the blooming of phytoplankton which form the base of the Arctic marine food web is an early phenomenon that depends on the availability of sunlight. In this study we argue that sunlight alone is not enough to drive large plankton blooms in the open ocean: an influx from sea ice meltwater is also needed. This meltwater (which is fresh and light) acts to maintain an ocean surface layer that is thin and separated from the ocean below. The plankton are confined to this surface layer where they can absorb plentiful sunlight and grow into large blooms. Here, we present an idealized model that describes this important role of sea ice meltwater for the growth of Arctic phytoplankton.

1 Introduction

Springtime in the Arctic Ocean is marked by large-scale algal growth events, known as phytoplankton blooms. In certain regions of the Arctic there has recently been an increase in the intensity of phytoplankton blooms (Lewis et al., 2020; Cherkasheva et al., 2014), with this increase being particularly notable near the Arctic sea-ice edge. During typical winter-spring transitions, the sympagic sea-ice edge environment is populated by algae communities that, under favorable conditions, grow rapidly into blooms (Leu et al., 2015). The magnitude and spread of these blooms depend on the availability of nutrients and sunlight, among other factors. In the spring, increased solar irradiance in the Arctic not only provides sunlight for photosynthesis, but also increases the melting of sea ice. Although it is typically nutritionally sparse, meltwater creates a stably stratified ocean-surface layer that constrains phytoplankton in the euphotic zone, making it a key factor in bloom development (Cherkasheva et al., 2014; Waniek et al., 2005; Janout et al., 2016; Mayot et al., 2018, 2020). This is supported by Landsat 8 satellite imagery which shows strong spatial correlations between phytoplankton blooms and low sea surface temperature (Figure 1), an indicator for meltwater concentration.

Phytoplankton form the base of the trophic food web and their blooms constitute a key component in the seasonal cycle of the Arctic ecosystem (Wassmann & Reigstad, 2011; Behrenfeld & Boss, 2014; Leu et al., 2015). Blooms also impact ocean-atmosphere dynamics through primary production and associated carbon dioxide uptake (Wassmann & Reigstad, 2011). Concerns about future changes in sea-ice cover and its role in altering spring bloom dynamics have further motivated recent field efforts (Cherkasheva et al., 2014; Arrigo & van Dijken, 2015). Although such observations and the satellite images of Figure 1 suggest a link between phytoplankton blooms and sea-ice melt, a dynamical understanding of the role meltwater plays in sea-ice edge phytoplankton blooms remains elusive.

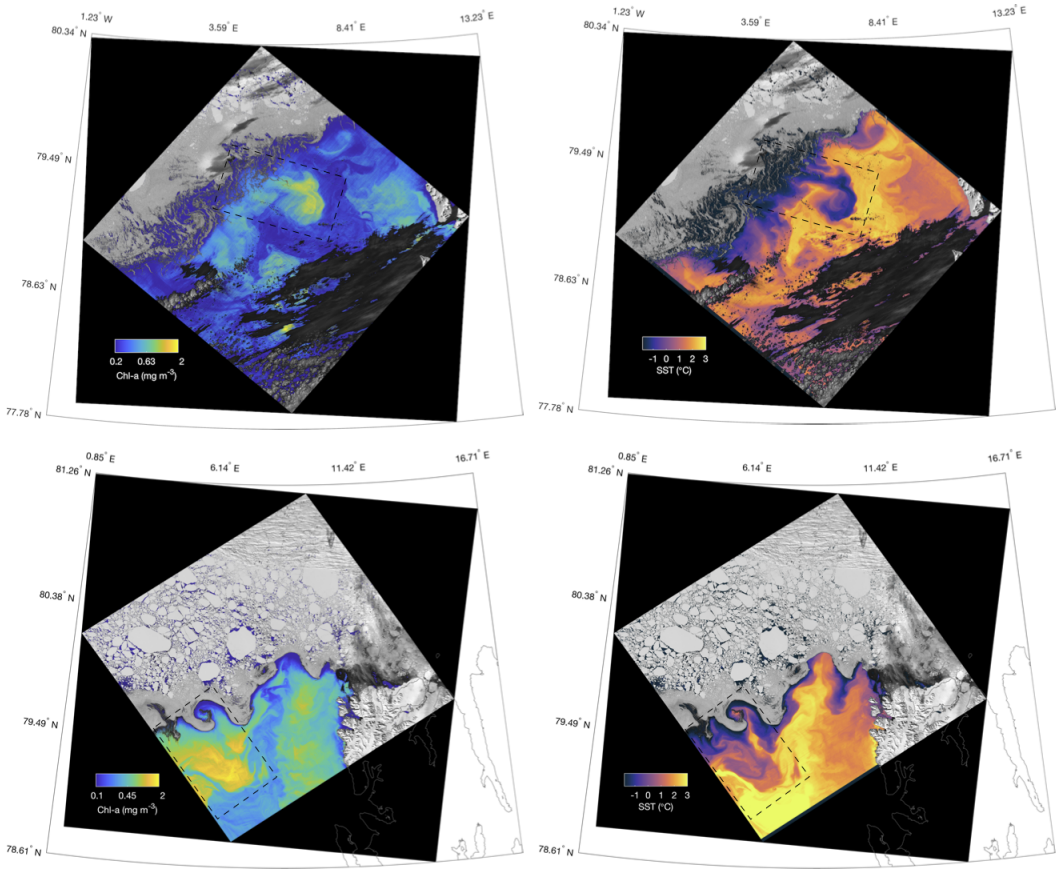

Figure 1. Landsat 8 images of a developing ice edge phytoplankton bloom taken in Fram Strait (sea ice is shown in grey/white). Svalbard is seen in the far right of both images. Left column shows chlorophyll-a (mg/m^3), right column SST (°C). Top: May 26,2019. Bottom: May 30, 2019. Bloom regions used in subsequent analysis outlined with dashed boxes.

Phytoplankton blooms are thought to occur when the surface mixed layer shoals to a critical depth in the spring, or when turbulent mixing at the surface is insufficient to remove the plankton from the surface (Behrenfeld & Boss, 2014). Stratification of the upper ocean due to meltwater from sea ice may therefore play a central role in determining whether a bloom is initiated and how large it will grow. This hypothesis is supported by anecdotal observational evidence of striking correlation between blooms and meltwater (Figure 1 and Cherkasheva et al., 2014; Wassmann & Reigstad, 2011; Mayot et al., 2020).

Beyond the central role of the mixed layer, bloom dynamics are controlled by grazing pressure from zooplankton and nutrient availability (Truscott & Brindley, 1994; Huppert et al., 2002; Behrenfeld & Boss, 2014). We note that blooms near the marginal ice zone may not be nutrient limited in the early spring as recent winter ice growth and associated salt rejection drive vertical convection and upward-mixing of nutrients (Mayot et al., 2018).

In this study we consider the role of sea ice meltwater for phytoplankton blooms near the ice edge. We develop an idealized model that accounts for plankton death and growth rates in a way that is physically motivated by the influence of meltwater and sunlight availability. The model builds on previous work using the Fisher reaction-diffusion

equation as a representation of open-ocean plankton dynamics (Birch et al., 2007). Specifically, we parameterize the role of meltwater and associated surface stratification which retains phytoplankton in the euphotic zone and thus provides enhanced growing conditions near the ice edge.

2 Plankton Model

Birch et al. (2007) simulated phytoplankton dynamics using the Fisher equation (Fisher, 1937; Kolmogorov et al., 1937) with a spatially variable growth rate and an incompressible velocity field. Their model can be presented as:

$$P_t + \mathbf{u} \cdot \nabla P = \gamma(\mathbf{x})P - \nu P^2 + \kappa \nabla^2 P, \tag{1}$$

where $P(\mathbf{x}, t)$ is phytoplankton concentration, $\mathbf{u}$ is the velocity field, $\gamma(\mathbf{x})$ is a spatially variable growth rate, ν is a constant death rate, and κ is a constant diffusivity.

Birch et al. (2007) present equation (1) in the context of open-ocean plankton dynamics with the goal of deriving bounds on total plankton biomass. The model as presented by Birch et al. (2007) has no explicit dependencies on nutrient limitations or grazing pressure. Nonetheless, plankton are able to reach a nontrivial steady state with rich transient dynamics dependent on stirring magnitude $|\mathbf{u}|$ and diffusivity κ.

Here, we modify equation (1) to study the dependence of phytoplankton blooms on meltwater near a sea-ice edge. To simulate phytoplankton-meltwater dynamics we include space and time dependence for the death rate ν in equation (1). Our hypothesis is that ν broadly reflects the effects that meltwater has on phytoplankton bloom development, namely that when meltwater is concentrated the death rate is lowered as phytoplankton are kept near the surface. Unlike Birch et al. (2007), we consider a constant growth rate γ. The growth rate is related to sunlight availability, which is needed for photosynthesis. By setting it constant we assume that the change in light availability over the duration of the simulation (i.e. the duration of a bloom) is small relative to other processes, such as changes in meltwater flux and plankton growth. With these modifications to equation (1), the model takes the form:

$$P_t + \mathbf{u} \cdot \boldsymbol{\nabla} P = \gamma P - \nu(\mathbf{x}, t)P^2 + \kappa \nabla^2 P, \tag{2}$$

$$\nu_t + \mathbf{u} \cdot \boldsymbol{\nabla} \nu = \alpha \nu + \kappa \nabla^2 \nu. \tag{3}$$

Equation (2) is equivalent to (1) aside from γ now being constant and $\nu(\mathbf{x}, t)$ varying in space and time (γ and ν only take positive values). Note that equation (2) and (3) contain the same velocity field $\mathbf{u}$ and diffusivity κ. This presupposes that phytoplankton are passive tracers which are advected and diffused at the same rate as the surface water in which they reside. The term $\alpha\nu$ in equation (3) causes exponential growth of ν (α is a positive constant). When ν reaches an upper bound, ν_{max}, we set $\alpha = 0$. The constant ν_{max} is interpreted as the open-ocean background death rate (without meltwater). $\alpha\nu$ can be interpreted as a proxy for wind-driven vertical mixing, where vertical mixing is suppressed near the ice edge and increases as you move away. From here forward we will refer to α as the vertical mixing rate.

We take the velocity field $\mathbf{u} = (u, v)$ to be the random two-dimensional field used by Birch et al. (2007), with slight modifications to mimic stirring at an ideal sea-ice edge;

$$\mathbf{u}(\mathbf{x}, t) = \begin{cases} U(c + (1-c)cos(k_m y + \phi_x),\ 0) & \text{for } n\tau \le t < (n+1/2)\tau, \\ U(c,\ cos(k_m x + \phi_y)) & \text{for } (n+1/2)\tau \le t < (n+1)\tau, \end{cases} \tag{4}$$

where $(x, y) \in [0, \ell)$. The velocity alternates between u and v on a given decorrelation time period τ with an imposed constant advection away from the ice edge of magnitude cU, such that space-time averages are $\langle u \rangle = cU$ and $\langle v \rangle = 0$. The positive constant c is added to insure mean advection away from the ice edge boundary; the wave number

$k_m = 2\pi m/\ell$, where ℓ is the domain length scale and ϕ_i is a phase shift randomly chosen between 0 and 2π each period.

In the subsequent analysis of the model, we will consider the nondimensional (*) versions of equations (2) and (3);

$$\frac{\partial P^*}{\partial t^*} + \mathbf{u}^* \cdot \boldsymbol{\nabla}^* P^* = P^* - \nu^* P^{*2} + k\nabla^{*2} P^*, \tag{5}$$

$$\frac{\partial \nu^*}{\partial t^*} + \mathbf{u}^* \cdot \boldsymbol{\nabla}^* \nu^* = \omega\nu^* + k\nabla^{*2} \nu^*, \tag{6}$$

with $P^* = P/K$, carrying capacity $K = \gamma/\nu_0$, $\nu^* = \nu/\nu_0$, and $\mathbf{u}^* = \mathbf{u}/(\gamma\ell)$. Space is scaled by the domain length ℓ and time by the biological growth time scale $1/\gamma$. This form highlights three characteristic dimensionless parameters controlling the model: *(i)* The Péclet number – the ratio of the diffusive time scale ℓ^2/κ to the advective time scale ℓ/U: Pe$\equiv U\ell/\kappa$; *(ii)* The Damköhler number – the ratio of the advective time scale to the biological growth time scale: Da $\equiv \gamma\ell/U$; *(iii)* The ratio of the vertical mixing rate α and sunlight–associated growth rate γ defined as: $\omega \equiv \alpha/\gamma$. The nondimensional diffusivity in (5) and (6) is $k \equiv 1/(\mathrm{Da}\,\mathrm{Pe}) = \kappa/\gamma\ell^2$.

Boundary conditions are applied to equations (5) and (6) that reflect sea-ice meltwater and phytoplankton conditions at and near the sea-ice edge at the beginning of the melt season. We supply the domain with a constant in-flux of low death rate ($\nu_0^* = 1$) and low phytoplankton concentration ($P_0^* = 0.05$) at $x^* = 0$. This in-flux is balanced by an equally constant out-flux at $x^* = 1$. The domain is thus non-periodic in x. The perpendicular boundaries are periodic at $y^* = (0, 1)$. A snapshot of a typical spun-up model output is seen in Figure 2. We initialize the model with the uniform background density $P^* = P_0^*$ and maximum death rate ν_{max}^* everywhere. In all simulations, $c = 0.5$ and $\nu_{max}^* = 20$. After several time steps a "bloom" develops near the in-flux boundary (the ice edge).

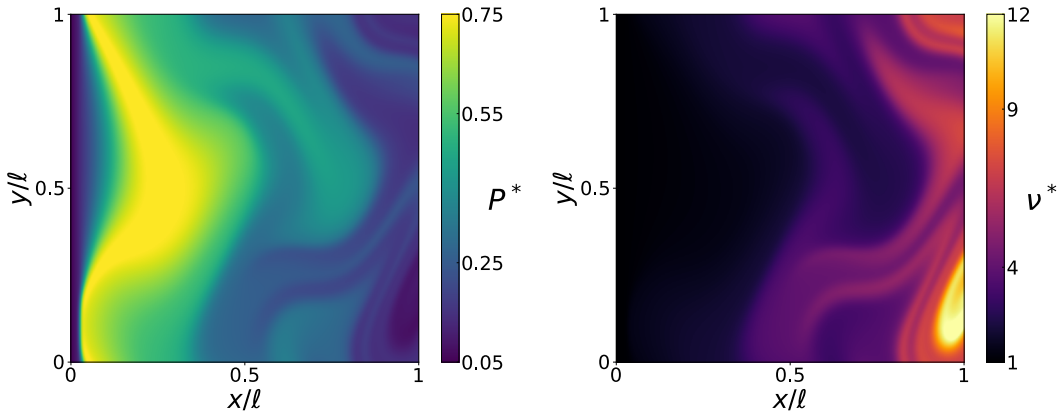

Figure 2. Snapshot of Model Output. Phytoplankton P^* (left) and death rate ν^* (right) are nondimensional. Here, $\mathrm{Da}^{-1} = 0.05,\ k = 5 \times 10^{-6},\ \tau = 10,\ \omega = 0.05$.

2.1 Limit of no horizontal diffusion

Here we consider environmental conditions where diffusive time scales are much larger than advective time scales (Pe $\to \infty$). To explore this limit we set $k = 0$ in equations (5) and (6). In this case, we can readily solve for the steady-state plankton concentration for a given advective field. Considering the idealized one-dimensional flow field $\mathbf{u}^* =$

$\langle \mathbf{u}^* \rangle = (\mathcal{U}, 0)$, where $\mathcal{U} \equiv cU/(\gamma\ell) = c/\mathrm{Da}$, the no-diffusion equivalents of equations (5) and (6) can be written as (dropping the nondimensional indicator (*) from here on):

$$\mathcal{U}\frac{dP}{dx} = P - \nu P^2, \tag{7}$$

$$\mathcal{U}\frac{d\nu}{dx} = \omega\nu. \tag{8}$$

This is solved to give plankton concentration as a function of distance from the ice edge x:

$$P(x) = \frac{e^{\frac{x}{\mathcal{U}}}}{\frac{1}{\omega+1}(e^{\frac{x}{\mathcal{U}}(\omega+1)} - 1) + \frac{1}{P_0}}. \tag{9}$$

We note that no bound is imposed on ν ($\alpha = 0$ for $\nu = \nu_{max}$ no longer applies) and $P \to 0$ as $\nu, x \to \infty$. This can be interpreted to mean the open-ocean background concentration of phytoplankton is zero.

The solution $P(x)$ in equation (9) highlights the spatial dynamics that may be expected of a bloom in this idealized environment. Namely, $P(x)$ has the intuitive shape of a heavy tailed distribution, where phytoplankton grow rapidly from a small initial value close to the ice edge boundary, peak, and decay slowly away from the ice edge. This "bloom curve" is sensitive to variations in the nondimensional parameters ω and Da^{-1} (Figure 3a,b). For instance, as ω (the ratio of vertical mixing to phytoplankton growth rate) gets larger the death rate increases more quickly with x, which reduces the bloom (Figure 3a). This can be interpreted as larger vertical mixing rates destabilizing and mixing the surface waters more efficiently, resulting in a less intense bloom. And as Da^{-1} (the ratio of the biological growth vs advective time scales) increases the bloom grows spatially, spanning a larger range in x, and its peak P_{max} is pushed further from the $x = 0$ boundary (Figure 3b). That is, a large in-flux of meltwater from the ice edge allows for a spatially large bloom to occur, peaking at a greater distance from the ice edge because of the increased advection speed.

3 Phytoplankton Meltwater Dependence

Equation (9) provides insight into the spatial behavior of an ice edge bloom subject to an idealized velocity field. However, when observing a real-world phytoplankton bloom (Figure 1) it is clear that the horizontal velocity field is highly complex, resulting in large fluctuations of phytoplankton concentration with distance from the ice edge. This renders $P(x)$ a suboptimal function to compare with data due to its strong dependence on the velocity field $\mathbf{u}$. We can, however, obtain another solution to equations (7) and (8) that is invariant of $\mathbf{u}$:

$$P(\nu) = \frac{\nu^{\frac{1}{\omega}}}{\frac{1}{\omega+1}(\nu^{\frac{1}{\omega}+1} - 1) + \frac{1}{P_0}}. \tag{10}$$

This solution represents the phytoplankton concentration as a function of death rate (meltwater) and produces a similar shaped "bloom curve" as $P(x)$ (Figure 3c,d). The velocity invariance of $P(\nu)$ is due to our initial assumption that phytoplankton are passive tracers and are advected at the same rate as the meltwater they reside in. Without the explicit dependence on horizontal mixing, $P(\nu)$ provides us with a framework in which we can qualitatively compare our model results to observational data (see below).

$P(\nu)$ is controlled by the parameter ω (Figure 3c). When ω is small (i.e., when vertical mixing is low) the phytoplankton maximum P_{max} is large at low values of ν. In the limit $\omega \to 0$ the death rate becomes spatially constant at $\nu_0 = 1$, allowing $P_{max} \to 1$.

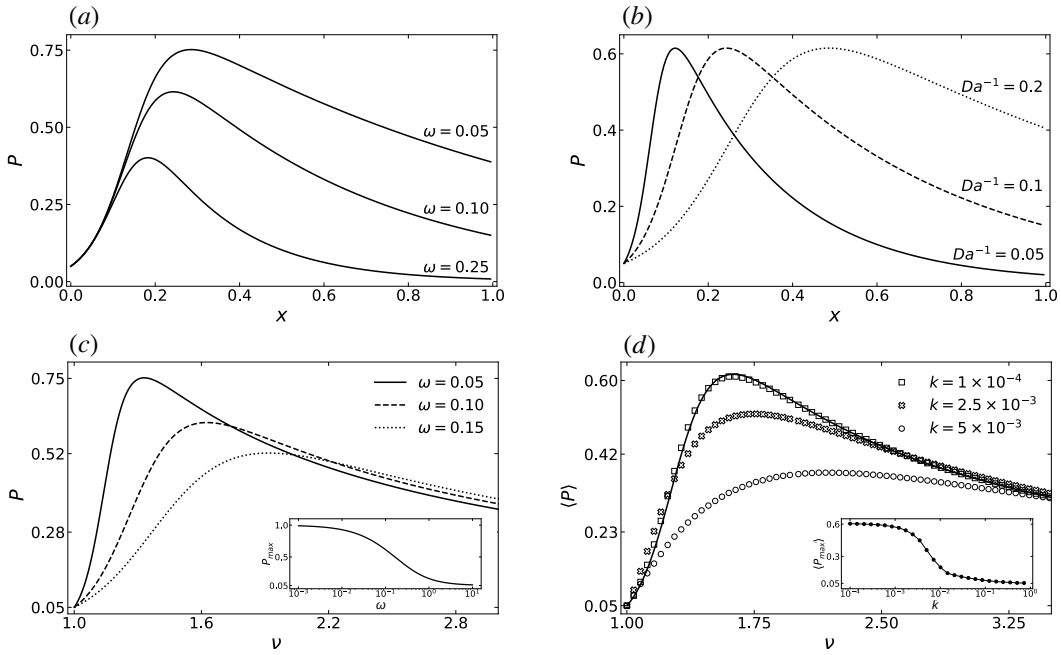

Figure 3. Top row: Phytoplankton concentration as a function of distance from the ice edge $P(x)$ on model parameters. (a) Analytic solutions of $P(x)$ for different values of ω. Here, $\mathrm{Da}^{-1} = 0.1$. (b) Analytic solutions of $P(x)$ with varying Da^{-1}. Here, $\omega = 0.1$. Bottom row: Phytoplankton concentration P as a function of death rate ν. (c) Analytic solutions of $P(\nu)$ in the limit of no diffusion (eq. 10), for different values of the characteristic growth rate ω. Inset: dependence of peak bloom value P_{max} on ω, with $P_{max} \to 1$ as $\omega \to 0$ and $P_{max} \to P_0$ as $\omega \to \infty$. (d) Numerical steady state solutions for the full model (eq. 5 and 6), for different values of diffusivity k. Solutions found by binning ν and averaging the P values in each bin, represented by $\langle P \rangle$. The analytic solution for $k = 0$ (eq. 10) is shown as the solid black line. Inset: P_{max} as a function of k, approaching P_0 as $k \to \infty$. Here, $\omega = 0.1$.

When ω is large (i.e., when vertical mixing is high) $\nu(P_{max})$ is pushed towards high values of ν and P_{max} is reduced, approaching P_0 everywhere in the limit $\omega \to \infty$.

To explore the influence of non-zero horizontal diffusion on the phytoplankton concentration we numerically solve equations (5) and (6) with varying values of k (Figure 3d). As expected, as diffusivity k increases the bloom peak P_{max} is increasingly suppressed. In the limit $k \to \infty$ the bloom peak vanishes as the plankton population in the domain homogenizes at P_0. In the limit $k \to 0$, on the other hand, the plankton bloom follows the zero-diffusivity curve described by the analytic solution above (eq. 10).

We note that equation (8) models the death rate as exponentially increasing with distance from the ice edge. This gives rise to the asymptotic decay in the phytoplankton concentration as ν grows large (Figure 3c,d). Qualitatively similar shapes for $P(\nu)$ to those in Figure 3 are found if the death rate ν increases in any fashion with x. That is, the "bloom curve" of $P(\nu)$ is present if equation (8) has the form: $\mathcal{U}\frac{d\nu}{dx} = f(\nu)$, with the conditions that $f(\nu) \geq 0$ and $f(\nu) = 0$ iff $\nu > \nu(P_{max})$.

Therefore, the particular spatial solution of equation (8), $\nu(x) \sim \exp(\omega x/\mathcal{U})$, represents just one possible functional form that is compatible with the observational data (see below). The physical interpretation here is that sea-ice meltwater is increasingly ver-

tically mixed out of the surface layer with distance from the ice edge; the exact spatial dependence of this mixing however is beyond the scope of this study.

3.1 Comparison to Observations

The modeled $P(\nu)$ (eq. 10, Figure 3c,d) suggest a dynamical interpretation of observed ice edge blooms (Figure 1). Because $P(\nu)$ is not dependent on horizontal mixing it provides a simple framework for us to interpret key bloom dynamics that may be present in bloom data – which we may expect to be approximately independent of horizontal stirring as well.

The images in Figure 1 are from high spatial resolution (30m) satellite imagery, taken May 26 and 30, 2019, by the NASA/USGS Landsat 8 mission in the Arctic region of Fram Strait. This imagery captures horizontal ocean surface data from the top several meters of the water column. We consider sea-surface temperature (SST) and chlorophyll-a (chl-a) as rough proxies for sea-surface meltwater and phytoplankton. Namely, low values of SST correspond to high meltwater concentration (low ν) and large values of chl-a to high phytoplankton concentration (high P).

To get at the relationship between phytoplankton and meltwater in the satellite data we compute binned averages of chl-a as a function of SST for the blooms in Figure 1 – considering only the regions experiencing an ice edge bloom, outlined by dashed boxes. The results (Figure 4) reveal two distinct regimes, present in both scenes: a positive correlation for low SST and a negative correlation for higher SST. In regions where SST is low and meltwater concentration high the positive correlation between chl-a and SST suggests that in this region the algae grow as they are transported away from the ice edge. In regions where SST is high (i.e., low meltwater concentration) the negative correlation between chl-a and SST suggests that the growth-favoring stratification is lost as meltwater is mixed vertically, and algae levels drop to a background value of chl-a present in the open ocean.

Note that both scenes in Figure 4 show similar mean chl-a concentrations ($\langle$chl-a$\rangle \approx 0.4\text{mg/m}^3$) at low SST (T$\approx -1.8°$C) near the ice edge. This suggests a relatively unchanged level of algae under the sea ice between May 26 and May 30. Similarly, the chl-a levels in the warm water limits are comparable for the two scenes ($\langle$chl-a$\rangle \approx 0.25-0.3\text{mg/m}^3$), indicating that this may be a "background" level of algae in the region at this time.

Because both scenes were taken in the same region only four days apart it is reasonable to assume that they represent different stages of the same regional bloom event. The earlier date (Figure 4, blue) shows the earlier, less developed stage while the later date (red) shows the more developed stage at which point the peak chl-a value has roughly doubled. The earlier scene exhibits its highest chl-a in rather cold waters (SST$\approx -1°$C) near the ice edge and an approximately linear increase of chl-a from the ice edge to this peak. As the bloom grows more mature, the positive correlation between meltwater and chl-a extends to SST$\approx 0°$C, which suggests that conditions are more advantageous for algae growth with increasing distance from the ice edge up to waters with 0°C. One explanation for this correlation is that the algae grow as they are advected away from the ice edge (by sub-mesoscale eddies, Figure 1) while confined to the meltwater-stratified shallow surface layer and exposed to an abundance of sunlight. The peak of the bloom therefore moves further into warmer waters and increases in maximum value.

The different slopes in the SST–chl-a relation for low SST ($< -.5°$C) between the two scenes may be (at least in part) due to differences in vertical mixing rates. A larger vertical mixing rate and weakened stratification in the later scene would explain the suppression of bloom growth (red curve), while the steeper slope for the earlier stage (blue curve) may indicate quiescent conditions with little vertical mixing and rapid algae growth.

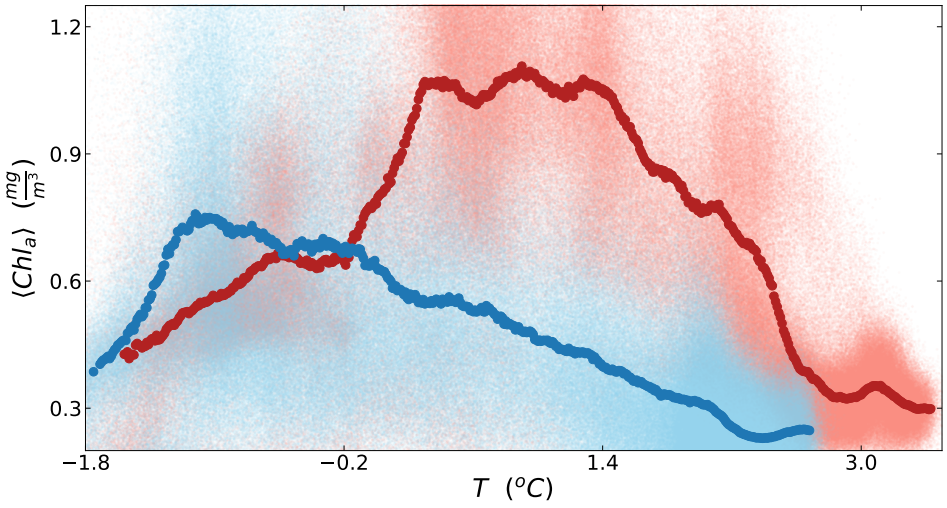

Figure 4. Observed chl-a vs SST from the regions outlined (dashed boxes) in Figure 1. Here, the data Landsat 8 image on May 26, 2019 is shown in blue and May 30, 2019 in red. The solid curves show averages of chl-a in SST bins (600 bins with width 0.01°C). Also plotted are 10^6 randomly selected pixels from each scene (blue and red point clouds). We ignore values of chl-a $< 0.16\text{mg/m}^3$ and $> 4\text{mg/m}^3$ and SST values < -1.8°C, which are likely satellite measurement anomalies. We note that the general shapes of the blue and red curves above are robust for different sized and oriented bounding boxes in Figure 1.

At the later stage of the bloom, conditions appear to be optimized for 0 <SST< 1.4°C, where peak ⟨chl-a⟩ concentrations are approximately constant at $\approx 1\ \text{mg m}^{-3}$. We note that from MODIS data (NASA Goddard Space Flight Center, 2018 Reprocessing) we estimate this bloom to be the largest May spring bloom in Fram Strait since MODIS started observing ocean surface color in 2002 (not shown).

For SST values higher than those at the chl-a peaks, we observe roughly linear decreases in chl-a in both cases which level off at $\approx 0.25 - 0.3\text{mg/m}^3$. This may be due to a loss of stratification with decreasing meltwater concentration in the surface layer. The steeper slope of the later stage may again indicate enhanced vertical mixing during that period.

The satellite-derived chl-a curves share similarities with major features in the model of $P(\nu)$ above (Figure 3c,d). As a bloom evolves in the model there is an initial growth phase at low ν associated with the in-flux of low phytoplankton concentration P_0 and low death rate ν_0 into the domain. This is analogous to the low chl-a and low SST values near the ice edge as seen in the data (Figures 1 and 4), where low SST indicates a meltwater-stratified shallow surface layer, associated with low phytoplankton death rate. Away from the model in-flux boundary, P and ν grow according to their respective growth rates, γ and α. In regions of high ν, the plankton concentration decays towards a steady-state value, the background plankton concentration. At an early stage of bloom evolution the bloom peak P_{max} is small and concentrated in regions of low ν. As the bloom intensifies P_{max} shifts towards higher values of ν, similar to the data (Figure 4).

From the analysis in Section 2.1 we know that bloom growth and intensity depends on the ratio $\gamma/\alpha \equiv \omega$ (eq. 10, Figure 3c). Namely, if ω is small – i.e. when the simulated death rate is small compared to the biological growth rate – $P(\nu)$ grows quickly in regions of low ν resulting in a more intense bloom, and if ω is large then $P(\nu)$ grows

slowly at low ν. This is in agreement with the interpretation above regarding the rate at which chl-a grows at low SST (Figure 4). However, our model only considers a constant vertical mixing rate α for a single bloom whereas our interpretation of the data above suggests that the vertical mixing rate may change substantially as the bloom evolves.

We note that the variations in chl-a growth at low SST in the data could also be a result of changes in phytoplankton growth rate. This could be caused, for example, by variations in sunlight availability. This effect can be captured by varying ω in our model. Namely, if the early stage of the bloom in the data (Figure 4, blue) is experiencing a larger growth rate γ, this would be analogous to decreasing ω. Lower ω in turn leads to a steep bloom growth at low ν, or in the case of the data, low SST. Equivalently, the later bloom stage (red) may be experiencing a smaller growth rate, therefore increasing ω in the model and resulting in less steep bloom growth at low ν (SST).

4 Conclusions and Discussion

We have presented an idealized model with a number of paramaterized dynamical processes to investigate spatial and temporal characteristics of phytoplankton blooms at the sea-ice edge. This builds on work by Birch et al. (2007), using a modified version of the Fisher equation. Our model results suggest that ice edge blooms can be characterized by two distinct regimes: *(i)* Growth near the ice edge – as the phytoplankton are advected away from the sea-ice edge and confined to a meltwater-stratified shallow surface layer, their growth is determined by the ratio of the biological growth rate and the rate of loss of stratification due to vertical mixing; *(ii)* Decay away from the ice edge – in regions beyond the peak bloom the phytoplankton concentration decreases together with the meltwater concentration, since a reduction in meltwater in the surface layer leads to weakened stratification and deeper vertical mixing of the plankton. Eventually, when the meltwater is well mixed the phytoplankton concentration returns to its background steady state levels present in the open-ocean.

The results from the idealized model presented here support a simple mechanism for how meltwater helps drive algae spring blooms near the marginal ice zone: During the spring melt period, the marginal sea-ice zone features a highly stratified cold and fresh surface layer that is maintained by meltwater in-flux and populated with sea-ice algae. Constrained in the euphotic zone by the melt, the algae grow rapidly by photosynthesis into a phytoplankton bloom near the ice edge. This mechanism suggests that blooms prosper in the stable environment provided by the sea-ice meltwater and are dynamically governed by meltwater concentration and sunlight availability. However, this mechanism may be limited to specific conditions. In particular, it assumes that the system is (at least initially) not nutrient limited. This can be the case early in the season after winter ice formation and corresponding brine rejection have driven vertical convection and enriched the ocean surface layer with nutrients. Ice edge blooms that occur later in the year may be substantially impacted by nutrient depletion as well as predation (Wassmann & Reigstad, 2011). We note that the assumption of no nutrient limitation may hold better in Eastern Fram Strait – the region covered by the satellite scenes – than in other regions. In this region warm Atlantic Water is advected from the subtropics and may contain the nutrients needed to facilitate bloom development. This warm northward current can additionally drive the bloom as it also accelerates sea-ice melt (Randelhoff et al., 2018).

The hierarchical importance of phytoplankton blooms for a thriving ecosystem in the Arctic is a driving motivator to understand how their dynamics vary with current and future variations in sea-ice conditions. As sea ice retreats further under global warming, the Arctic spring may eventually occur without sea ice. If this is the case, there would be no meltwater, and hence the possibility of drastically reduced phytoplankton spring blooms, causing radical changes to the Arctic ecosystem.

Acknowledgments

This work was supported by NSF OPP awards 1744835 and 1643445. Data used in this study (Landsat 8 scenes in Figure 1 and 4) were acquired via U.S. Geological Survey (USGS) Earth Explorer (https://earthexplorer.usgs.gov) and were processed using NASA SeaDAS (Baith et al., 2001). The authors thank Greenpeace for ship time and logistics support for the May 2019 field work during which this project was developed.

References

Arrigo, K. R., & van Dijken, G. L. (2015). Continued increases in arctic ocean primary production. *Progress in Oceanography*, *136*, 60–70.

Baith, K., Lindsay, R., Fu, G., & McClain, C. R. (2001). Data analysis system developed for ocean color satellite sensors. *Eos, Transactions American Geophysical Union*, *82*(18), 202–202.

Behrenfeld, M. J., & Boss, E. S. (2014). Resurrecting the ecological underpinnings of ocean plankton blooms.

Birch, D. A., Tsang, Y.-K., & Young, W. R. (2007). Bounding biomass in the fisher equation. *Physical Review E*, *75*(6), 066304.

Cherkasheva, A., Bracher, A., Melsheimer, C., Köberle, C., Gerdes, R., Nöthig, E.-M., ... Boetius, A. (2014). Influence of the physical environment on polar phytoplankton blooms: a case study in the fram strait. *Journal of Marine Systems*, *132*, 196–207.

Fisher, R. A. (1937). The wave of advance of advantageous genes. *Annals of eugenics*, *7*(4), 355–369.

Huppert, A., Blasius, B., & Stone, L. (2002). A model of phytoplankton blooms. *The American Naturalist*, *159*(2), 156–171.

Janout, M. A., Hölemann, J., Waite, A. M., Krumpen, T., von Appen, W.-J., & Martynov, F. (2016). Sea-ice retreat controls timing of summer plankton blooms in the eastern arctic ocean. *Geophysical Research Letters*, *43*(24), 12–493.

Kolmogorov, A., Petrovskii, I., & Piscunov, N. (1937). A study of the equation of diffusion with increase in the quantity of matter, and its application to a biological problem. *Byul. Moskovskogo Gos. Univ.*, *1*(6), 1–25.

Leu, E., Mundy, C., Assmy, P., Campbell, K., Gabrielsen, T., Gosselin, M., ... Gradinger, R. (2015). Arctic spring awakening–steering principles behind the phenology of vernal ice algal blooms. *Progress in Oceanography*, *139*, 151–170.

Lewis, K. M., van Dijken, G. L., & Arrigo, K. R. (2020). Changes in phytoplankton concentration now drive increased arctic ocean primary production. *Science*, *369*(6500), 198–202. Retrieved from `https://science.sciencemag.org/content/369/6500/198` doi: 10.1126/science.aay8380

Mayot, N., Matrai, P., Arjona, A., Bélanger, S., Marchese, C., Jaegler, T., ... Steele, M. (2020). Springtime export of arctic sea ice influences phytoplankton production in the greenland sea. *Journal of Geophysical Research: Oceans*, *125*(3), e2019JC015799.

Mayot, N., Matrai, P., Ellingsen, I., Steele, M., Johnson, K., Riser, S., & Swift, D. (2018). Assessing phytoplankton activities in the seasonal ice zone of the greenland sea over an annual cycle. *Journal of Geophysical Research: Oceans*, *123*(11), 8004–8025.

NASA Goddard Space Flight Center, O. B. P. G., Ocean Ecology Laboratory. (2018 Reprocessing). *Moderate-resolution imaging spectroradiometer (modis) aqua chlorophyll data.* (Accessed on 06/23/2020) doi: data/10.5067/AQUA/MODIS/L3B/CHL/2018

Randelhoff, A., Reigstad, M., Chierici, M., Sundfjord, A., Ivanov, V., Cape, M., ... Kristiansen, S. (2018). Seasonality of the physical and biogeochemical hy-

drography in the inflow to the arctic ocean through fram strait. *Frontiers in Marine Science*, *5*, 224.

Truscott, J., & Brindley, J. (1994). Ocean plankton populations as excitable media. *Bulletin of Mathematical Biology*, *56*(5), 981–998.

Waniek, J. J., Holliday, N., Davidson, R., Brown, L., & Henson, S. (2005). Freshwater control of onset and species composition of greenland shelf spring bloom. *Marine Ecology Progress Series*, *288*, 45–57.

Wassmann, P., & Reigstad, M. (2011). Future arctic ocean seasonal ice zones and implications for pelagic-benthic coupling. *Oceanography*, *24*(3), 220–231.

Figure 1.

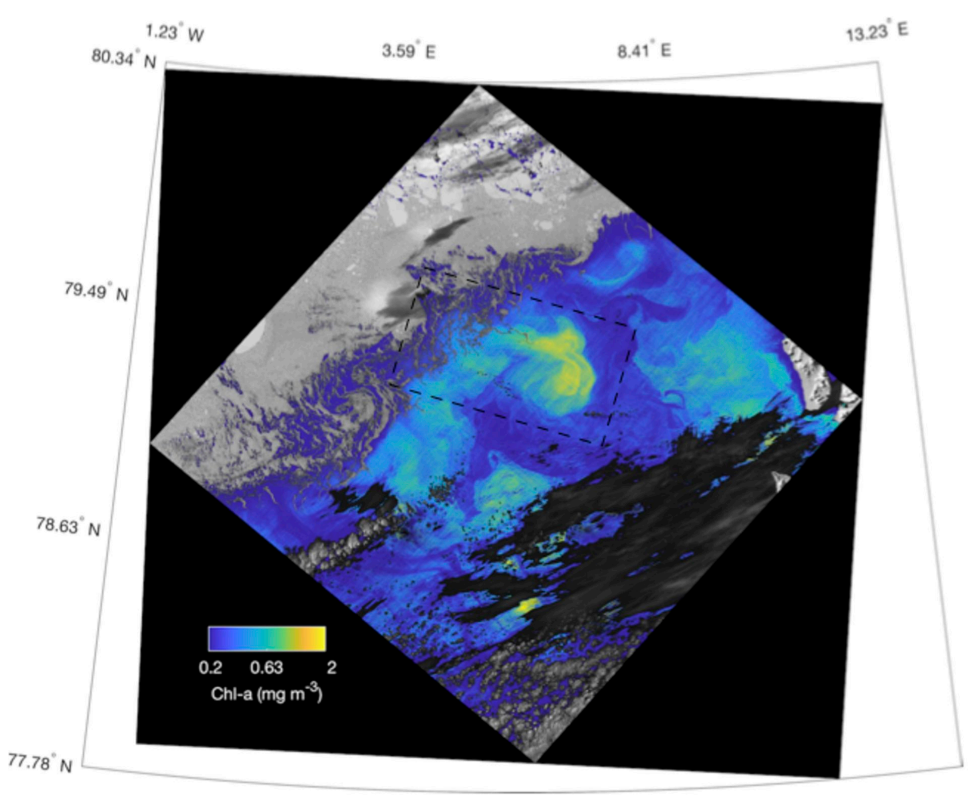
1.23° W
3.59° E
8.41° E
13.23° E
80.34° N
79.49° N
78.63° N
77.78° N
0.2 0.63 2
Chl-a (mg m-3)

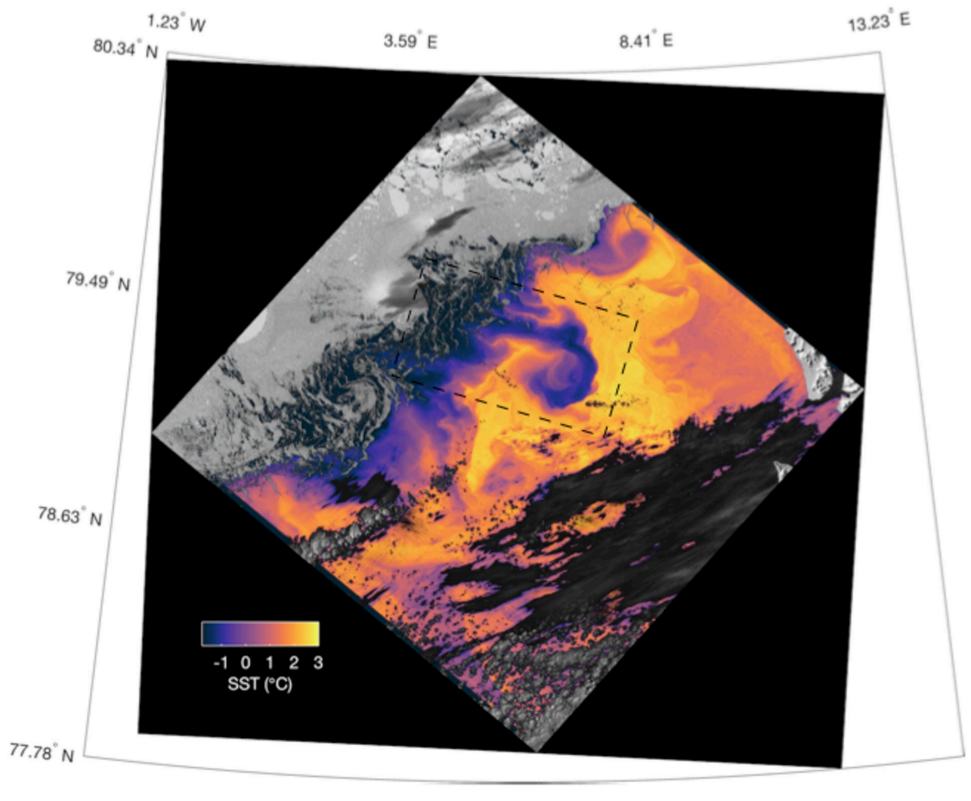
1.23° W
3.59° E
8.41° E
13.23° E
80.34° N
79.49° N
78.63° N
77.78° N
-1 0 1 2 3
SST (°C)

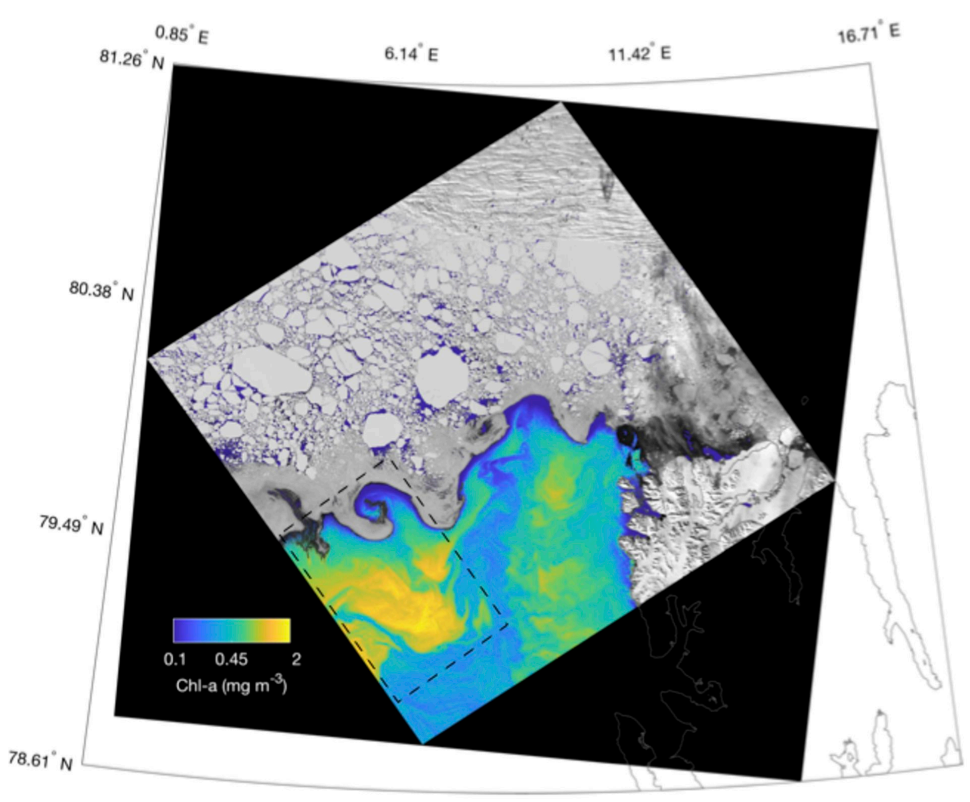
0.85° E
6.14° E
11.42° E
16.71° E
81.26° N
80.38° N
79.49° N
78.61° N
0.1 0.45 2
Chl-a (mg m-3)

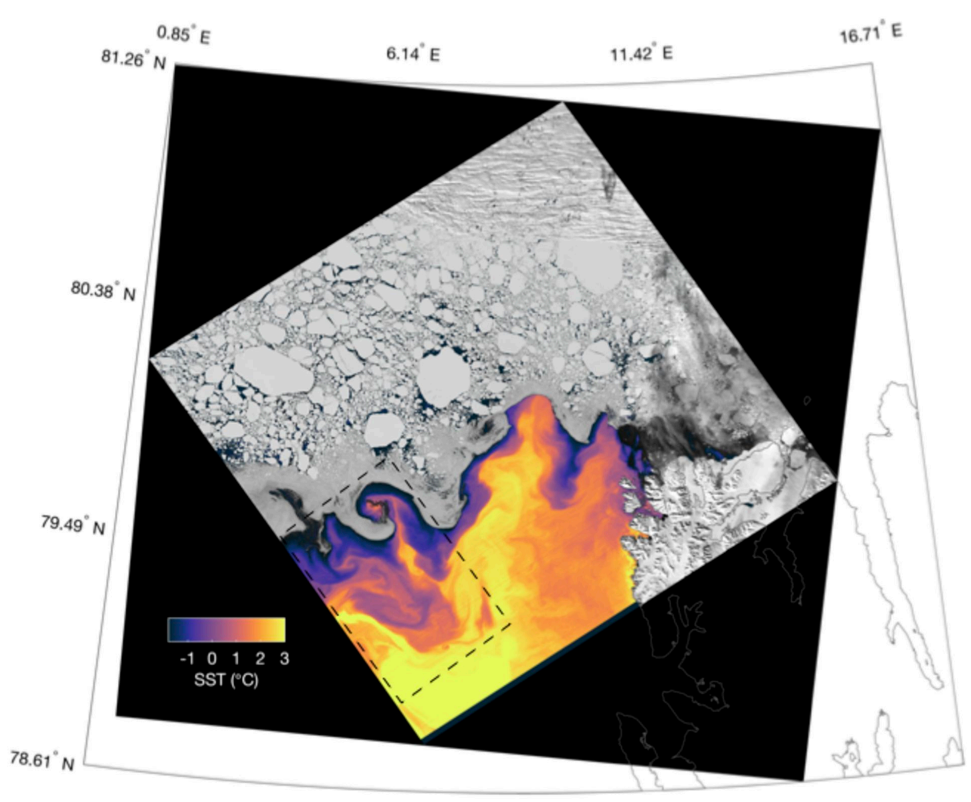
0.85° E
6.14° E
11.42° E
16.71° E
81.26° N
80.38° N
79.49° N
78.61° N
-1 0 1 2 3
SST (°C)

Figure 2.

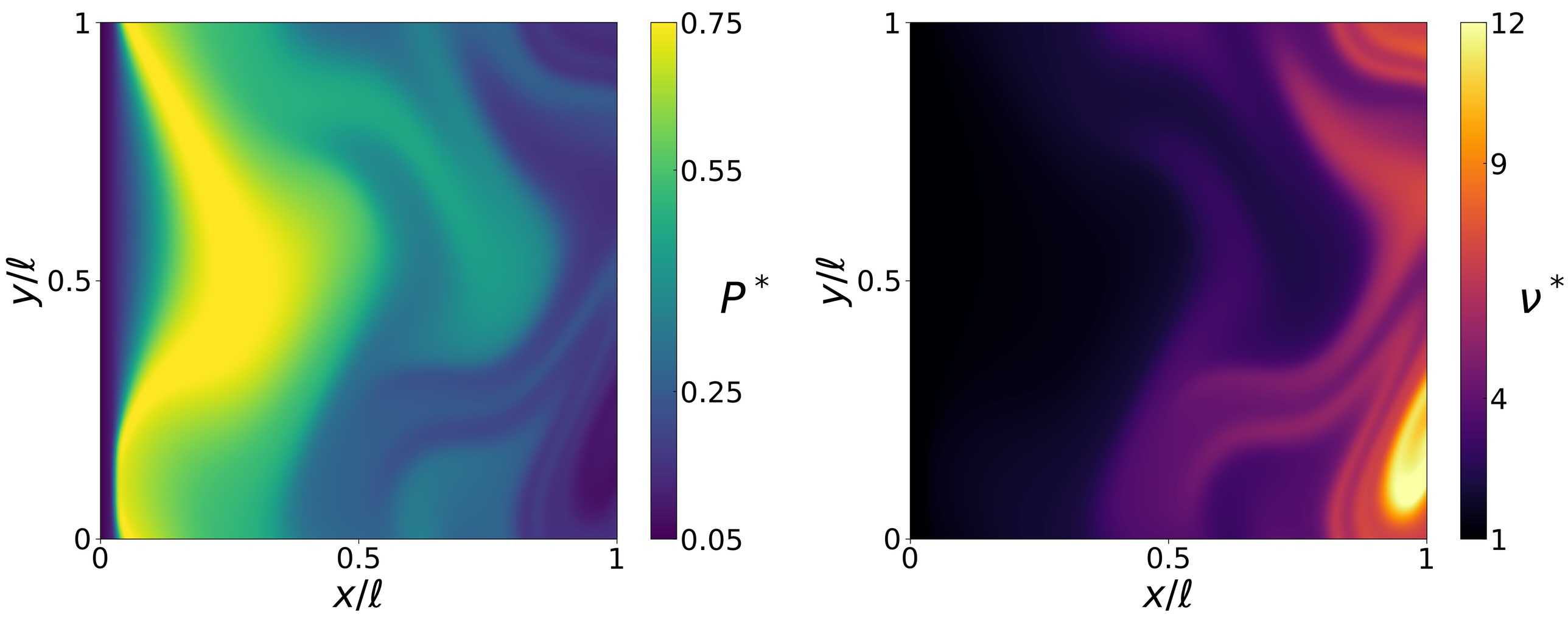
1
0.5
0
y/ℓ
0
0.5
1
x/ℓ
0.75
0.55
0.25
0.05
P*
1
0.5
0
y/ℓ
0
0.5
1
x/ℓ
12
9
4
1
ν*

Figure 3.

(a)

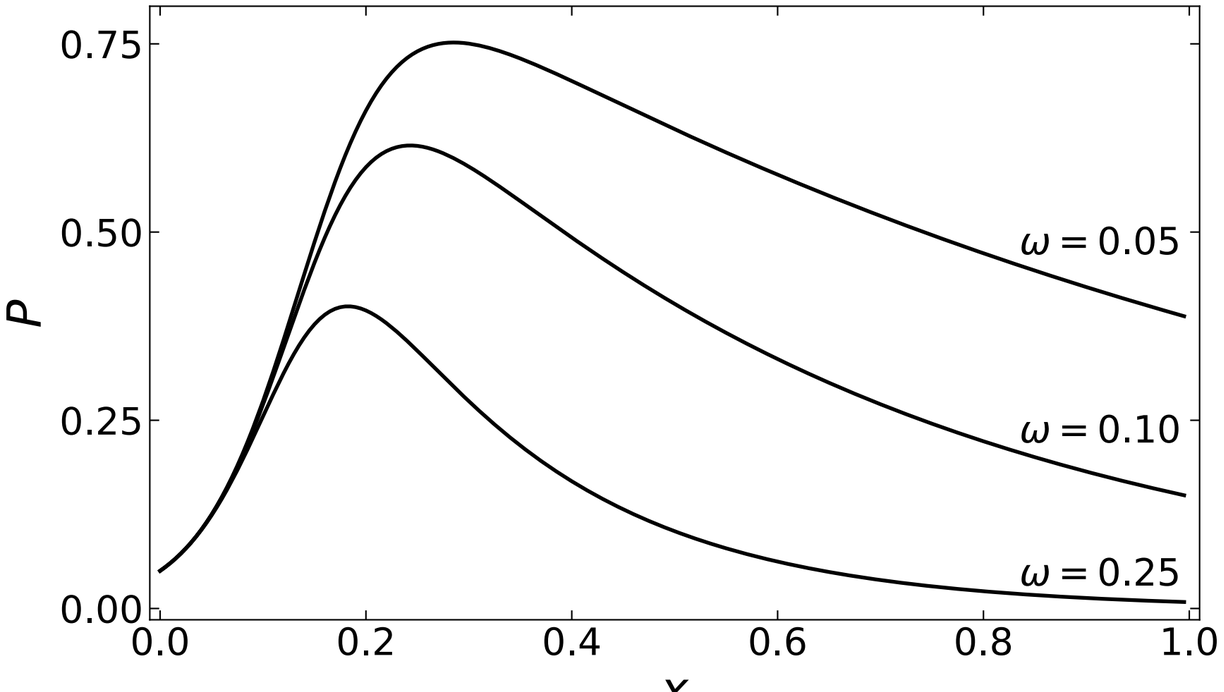
0.75
0.50
0.25
0.00
P
0.0
0.2
0.4
0.6
0.8
1.0
x
ω = 0.05
ω = 0.10
ω = 0.25

(b)

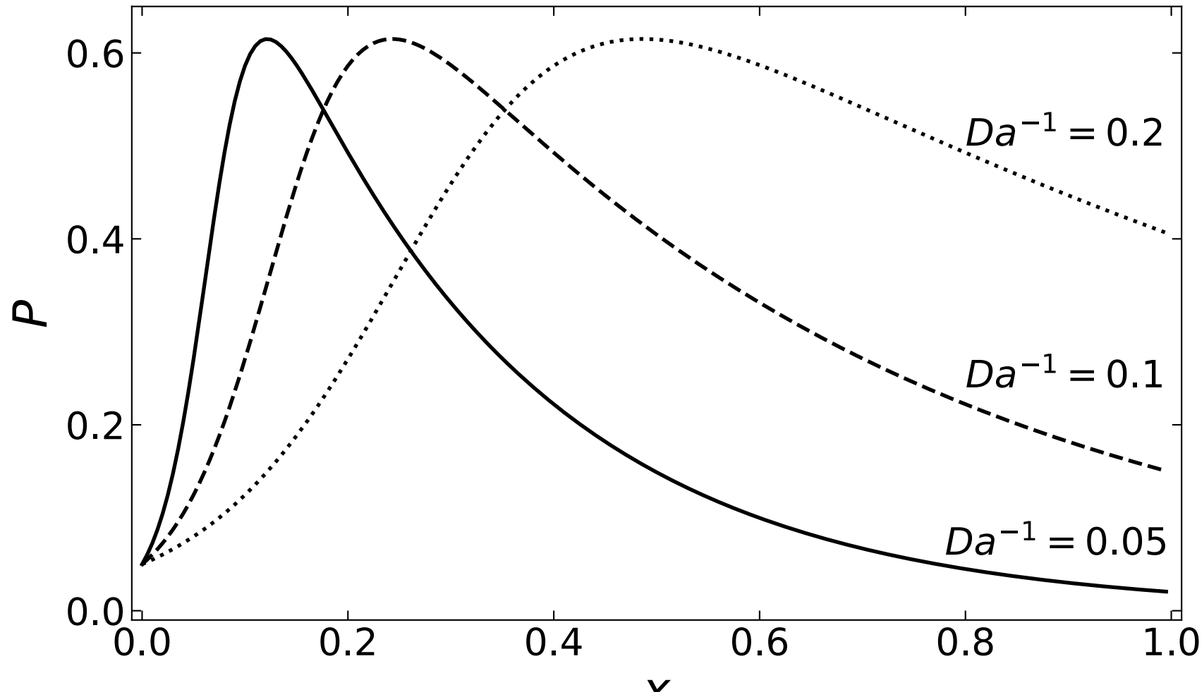
0.6
0.4
0.2
0.0
P
0.0
0.2
0.4
0.6
0.8
1.0
x
Da⁻¹ = 0.2
Da⁻¹ = 0.1
Da⁻¹ = 0.05

(c)

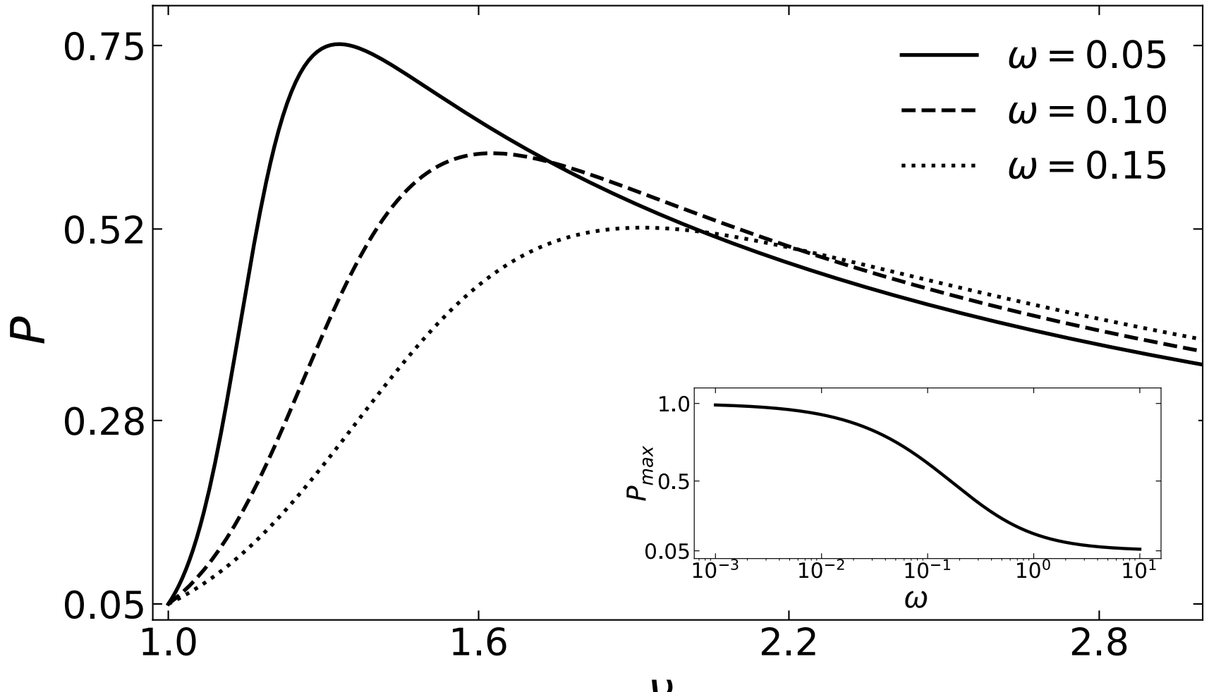
0.75
0.52
0.28
0.05
P
1.0
1.6
2.2
2.8
ν
ω = 0.05
ω = 0.10
ω = 0.15
P_max
1.0
0.5
0.05
10⁻³
10⁻²
10⁻¹
10⁰
10¹
ω

(d)

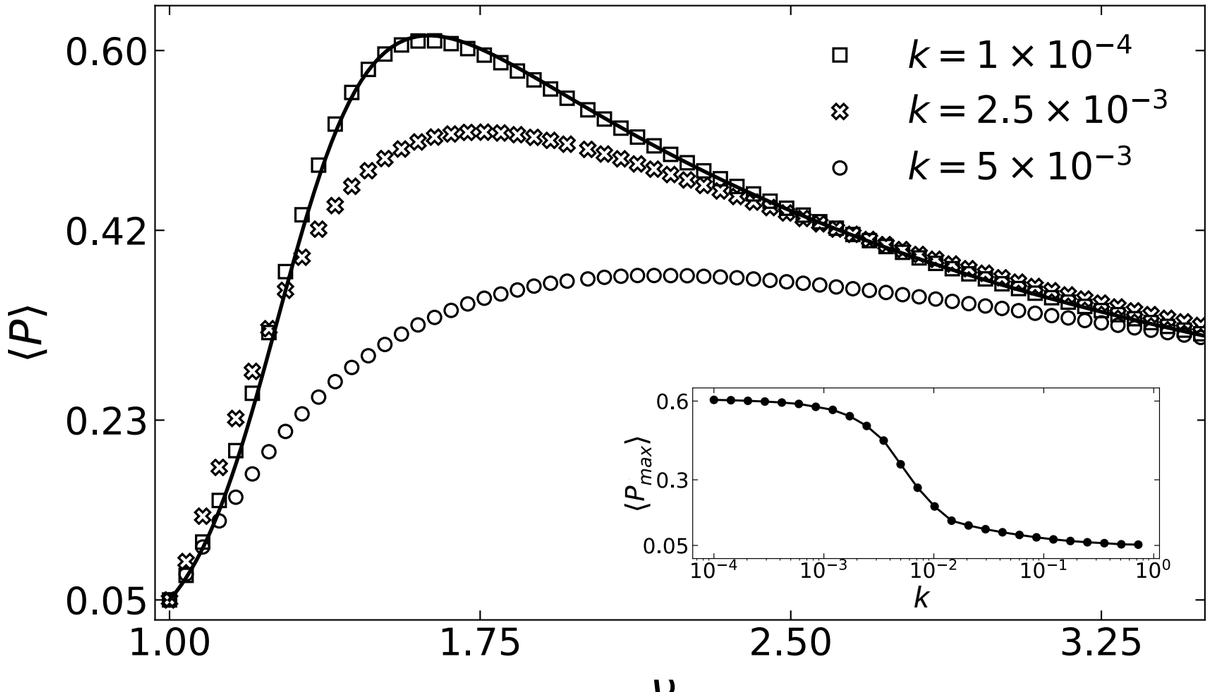
0.60
0.42
0.23
0.05
⟨P⟩
1.00
1.75
2.50
3.25
ν
k = 1 × 10⁻⁴
k = 2.5 × 10⁻³
k = 5 × 10⁻³
⟨P_max⟩
0.6
0.3
0.05
10⁻⁴
10⁻³
10⁻²
10⁻¹
10⁰
k

Figure 4.

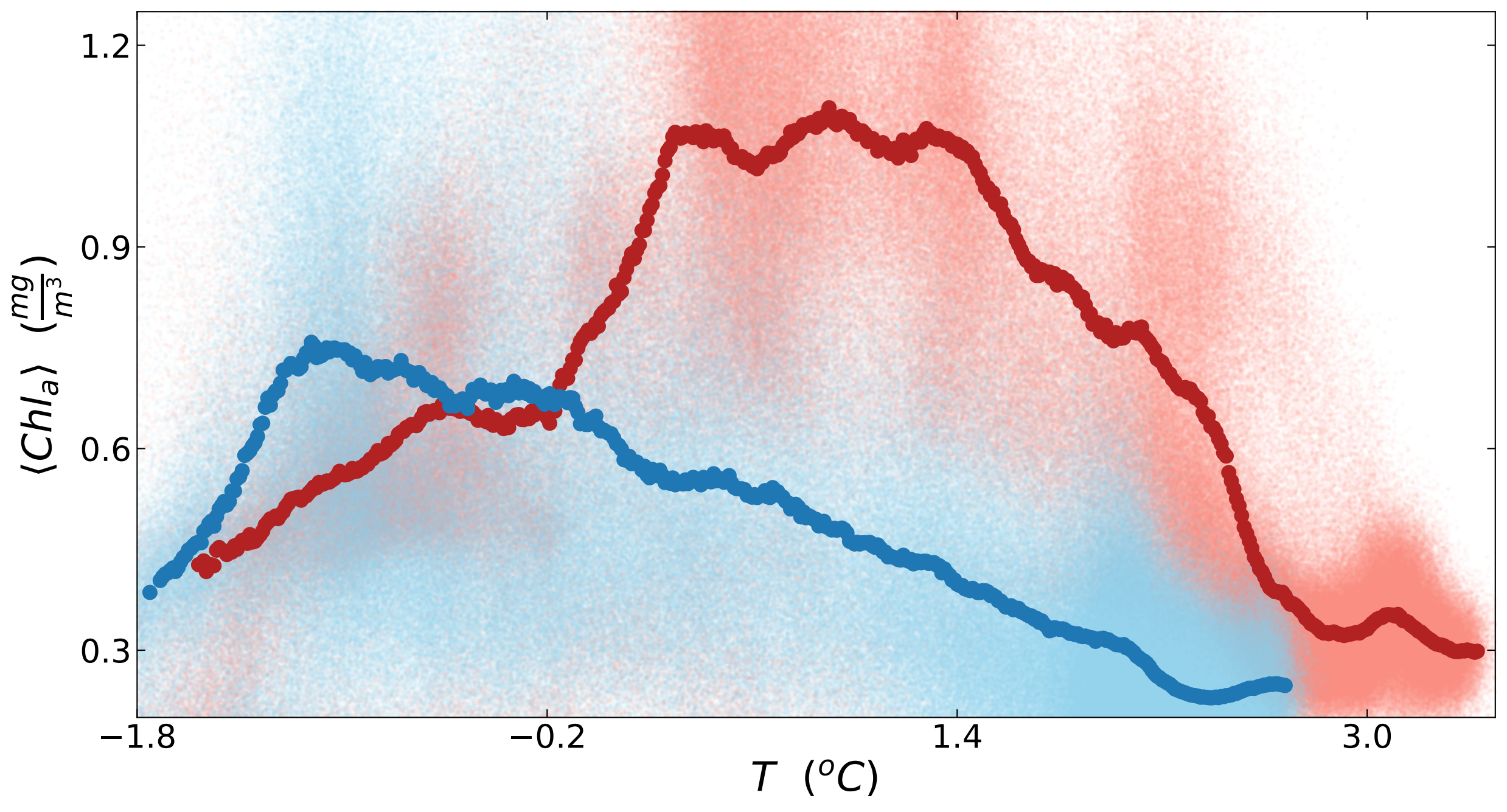
1.2
0.9
0.6
0.3
$\langle Chl_a \rangle$ $(\frac{mg}{m^3})$
−1.8
−0.2
1.4
3.0
T (^oC)